Journal of Applied Polymer Science

# Temperature Sensitivities of Doped Polyaniline Nanoscale Films on Flexible Substrates

**Hakeem Abrar Ahmad,[1,2] Debabrata Nayak,[1,2] Siddhartha Panda[1,2]**

[1]Department of Chemical Engineering, Indian Institute of Technology Kanpur, Kanpur, Uttar Pradesh 208016, India

[2]Samtel Centre for Display Technologies, Indian Institute of Technology Kanpur, Kanpur, Uttar Pradesh 208016, India

Correspondence to: S. Panda (E-mail: spanda@iitk.ac.in)

**ABSTRACT:** There is a need to develop more sensitive and cheaper flexible temperature sensors and sensor arrays. In this work, sub-100-nm thick polyaniline films of different thicknesses and doping content, coated on flexible PET substrates were used to study the temperature sensing behavior. The material and electrical properties of the films were characterized. The temperature sensitivities, based on DC measurements, varied with the film thickness and the doping content, with the variations being more pronounced at lower thicknesses. Higher sensitivities were obtained with thinner films at lower doping levels and these values are significantly higher than those obtained in commercially available flexible temperature sensors and moreover, these sensitivities could be tuned over a wider range. A possible mechanism was proposed to explain the experimental results, which was supported by the values of the calculated phonon frequencies. AC studies were conducted to identify the transport mechanisms and the transport parameters were calculated. An optimum window of conductivity was needed to obtain high sensitivities and the sensitivities could be tuned by varying the film thickness and the doping content. These films did not show discernable change in resistance upon bending and could be used on curved surfaces. © 2012 Wiley Periodicals, Inc. J. Appl. Polym. Sci. 129: 230–237, 2013

**KEYWORDS:** sensors and actuators; nanostructured polymers; conducting polymers

Received 13 July 2012; accepted 13 October 2012; published online 6 November 2012

**DOI: 10.1002/app.38720**

## INTRODUCTION

Measurement of temperature distributions on curved surfaces is needed in several areas such as electronic appliances, aerodynamics, automobiles, and medicine. This is achieved by use of flexible temperature sensors and sensor arrays. The current sensor arrays use silicon[1] or thin metal strips[2,3] as sensing elements on a flexible polymer substrate such as polyimide. Use of silicon sensing elements requires several expensive processing steps normally associated with silicon processing, and silicon etchants are known to have a deleterious effect on the polymer substrates. Similarly, metal deposition often requires expensive consumables. Along with higher costs, there is a critical shortcoming—reliability, due to mismatch of thermal expansion between the semiconductor/metal sensing element and the polymer substrate[3] which also restricts the temperature range of operation. Temperatures are also measured by thermochromic films where temperature changes are observed by a change in color. However, these are relatively expensive and the color range is limited. Hence there is need to develop cheaper and more reliable flexible temperature sensors and sensor arrays. For this, cheap materials and simpler (and hence cheaper) processes need to be developed. One such class of materials is conducting polymers, and in this work, thin (sub-100 nm) films of polyaniline doped with camphorsulfonic acid (PANI CSA) are used as sensing elements on flexible polyethylene terephthalate (PET) substrates.

The published works on the dependences of the electrical conductivity of polyaniline on temperature include use of different forms of the polyaniline sensing elements (drop-cast films or pellets), different dopants and different blends. It is to be noted that the literature review provided below is representative and not exhaustive. Kim et al.[4] studied the temperature-dependent electrical conductivity of pellets (500-$\mu$m thick) of polyaniline doped with dodecylbenzene sulfonic acid (PANI DBSA) and polyaniline doped with hydrochloric acid (PANI HCl), in the temperature range 298–498 K. The conductivity increased and then decreased with temperature which was attributed to thermal assisted protonation and deprotonation. Long et al.[5] made composite drop cast films of PANI CSA and PANI DBSA (film thickness not reported) and reported a change in the temperature coefficient of resistance from negative to positive in the temperature range 120–300 K. Ebrahim et al.[6] measured the DC and AC temperature dependent conductivity of cast films

(thickness not provided) of polyaniline/polyvinyl formal blends with different weight percentages of PANI in the range 100–300 K. The DC conductivity followed the variable range hopping (VRH) behavior while the AC conductivity was described by correlated barrier hopping (CBH). Pinto et al.[7] studied the temperature-dependent resistance behavior of PANI doped by 2-acrylamido-2-methyl-1-propanesulfonic acid (PANI AMPSA) drop cast films (15-$\mu$m thick) and pellets and the responses were attributed to the role of the solvent induced structural order in the polymer. Prakash et al.[8] studied temperature-dependant resistance measurement of PANI CSA drop cast films (1.4–5.9 $\mu$m thick) and reported nonlinear temperature coefficients of resistance. Huang et al.[9] studied the temperature dependence of conductivity of tubular and granular PANI doped by $\beta$-naphthalenesulfonic acid (PANI NSA) in the range 77—300 K (film thicknesses not provided). The materials showed a negative temperature coefficient of resistance and a one-dimensional VRH behavior was observed. Bhadra and Sarkar[10] synthesized polyaniline nanorods (100–500 nm) in polyvinyl alcohol (PVA) and the cast PANI-PVA film (thickness not provided) had a two-dimensional hopping behavior in the temperature range of 93–300 K. Dutta et al.[11] reported the DC and AC conductivity values of cast PANI–PVA blend films (thickness not provided) in the temperature range of 80 K to room temperature. The DC conductivity was explained by the VRH behavior while the AC conductivity followed the CBH model. Gupta et al.[12] reported the temperature variation (77–300 K) of DC conductivity of pellets (dimensions not mentioned) of composites of PANI nanorods and $CuCl_2$ by the quasi-one-dimensional hopping model and tunneling model while that of the AC conductivity was explained by the CBH model. Sarkar et al.[13] reported the DC and AC conductivity of cast films (thickness not provided) of doped PANI-methyl cellulose blends dispersed in PVA in the temperature range 77–300 K. The DC conductivity was explained by hopping transport between the superlocalized states and the AC conductivity was explained by the CBH behavior. Bianchi et al.[14] reported the AC conductivity of polyaniline films (12-$\mu$m thick) which were explained by the random free energy barrier model. Nazeer et al.,[15] reported solution cast polyaniline films (9.8-$\mu$m thick) to follow the 3D VRH mechanism based on DC measurements and the overlapping large polaron tunneling mechanism based on AC measurements. Adams et al.[16] reported the conductivity of PANI AMPSA films (thickness not provided) in the temperature range 15–300 K and showed a transition from a negative coefficient of resistance to a positive coefficient of resistance with the transition temperature being a function of the doping content.

As seen above, the temperature sensitivity studies on doped PANI and PANI blends have done been mostly on samples (films, pellets) whose thicknesses are in the micron range or higher. There is limited work[17,18] on the study of these films in the sub-100-nm range. Jin et al.[17] characterized the electrical and thermal conductivities of 55-nm-thick spin-coated polyaniline (PANI) films doped with different levels of CSA coated on silicon dioxide substrates. The maximum electrical conductivity of the film reported was about 65 S $cm^{-1}$ at about 60% (the molar ratio of CSA to phenyl-*N* repeat unit of PANI) doping level. Jin et al.,[18] in another paper, reported 500 and 200% increase in the in-plane thermal conductivity and electrical conductivity, respectively, as the PANI CSA film thickness was increased from 20 to 1000 nm. Again, these papers did not report the temperature sensitivity studies. To the best of our knowledge, we are not aware of any temperature sensitivity studies on doped polyaniline films in the sub-100 nm regime. In the present work, the effects of physical dimensions of the sub-100 nm films and chemical composition (i.e., doping level) on the temperature sensitivities of these PANI-CSA films spin-coated on flexible PET substrates are reported. The transport parameters are calculated from the DC and AC conductivity measurements and possible mechanisms for the observed behaviors are proposed. The temperature sensitivities obtained from this work are compared with those obtained in commercially available flexible temperature sensors.

## EXPERIMENTAL

### Material and Film Preparation

Polyaniline emeraladine base (PANI EB) was prepared by chemical oxidative polymerization of aniline (Rankem) in presence of HCl (Fisher Scientific) by using aqueous solution of ammonium persulfate (APS) (Fisher Scientific).[19] Solution of aniline in 1*M* aqueous HCl was cooled below 5°C in an ice bath. Aqueous solution of APS was then added drop wise over a period of 1 h to the above solution under vigorous stirring. The precipitate formed was collected by filtration and then washed repeatedly with 1*M* aqueous HCl to remove the residual monomer and oxidant until the filtrate was colorless. A very dark greenish precipitate was obtained which provided visual confirmation of the HCl doped PANI. The HCl doped PANI was converted to PANI EB by treatment with 1*M* aqueous $NH_4OH$ for 4 h and then was washed to neutral with deionized water. A final washing with acetone removed the low-molecular-weight organic intermediates and oligomers and prevented the aggregation of the PANI precipitate during drying. Then the PANI EB powder was dried in a vacuum oven (−700 mmHg) for 48 h at 60°C.

PANI EB was doped with different quantities of CSA (Merck). Three different samples of doped polymers were prepared by using 0.5 g of PANI EB: with 0.3, 0.5, and 1 g of CSA, respectively. These three samples were indicated by $(PANI\ CSA)_{0.6}$, $(PANI\ CSA)_{1.0,}$ and $(PANI\ CSA)_{2.0,}$ respectively and are also referred to having doping ratios of 0.6, 1.0, and 2.0, respectively. The doping was done in *m*-cresol solvent by keeping the mixture stirred for about 6 h and using an appropriate volume of solvent. The mixture was sonicated for 15 min and then kept undisturbed about an hour for the heavy insoluble particles to settle down and then centrifuged (at 10,000 rpm) for 10 min to remove any suspended particles. The solution was ready to be used for spin coating on the substrates. The polymer solution obtained in the *m*-cresol was spin coated on square (2.5 cm × 2.5 cm) PET substrates (180-$\mu$m thick) at different rotation speeds using a spin coater (Apex Instruments, India). The films were then dried at 60°C in a vacuum oven (at −700 mmHg) for 2 h. Copper strips (2.5 cm × 0.2 cm) were used as contacts.

**Table I.** Measured Film Properties and Transport Parameters Calculated from AC Measurements for (a) $(PANI\ CSA)_{0.6}$ Films (b) $(PANI\ CSA)_{1.0}$ Films (c) $(PANI\ CSA)_{2.0}$ Films

| | | | Calculated AC parameters at 1 MHz | | | |
|---|---|---|---|---|---|---|
| | Experimental | | In the range 303–353 K | | At 303 K | |
| Sample | Thickness (nm) | $\sigma$ (S cm$^1$) at 1 MHz | $W_H$ (eV) | $\tau_0$ (s) | $R_\omega$ (nm) | $N(E_F)$ (/eV cm$^3$) |
| $(PANI\ CSA)_{0.6}$ | 75 ± 3.4 | 6.909 | 0.066 | $6.02 \times 10^{-11}$ | 2.94 | $2.71 \times 10^{23}$ |
| | 49 ± 3.0 | 4.557 | 0.091 | $2.34 \times 10^{-11}$ | 2.94 | $2.20 \times 10^{23}$ |
| | 23.6 ± 2.0 | 3.977 | 0.099 | $1.67 \times 10^{-11}$ | 2.95 | $2.04 \times 10^{23}$ |
| $(PANI\ CSA)_{1.0}$ | 64 ± 0.5 | 11.422 | 0.046 | $27.73 \times 10^{-11}$ | 2.52 | $4.74 \times 10^{23}$ |
| | 56 ± 1.4 | 10.714 | 0.063 | $9.01 \times 10^{-11}$ | 2.78 | $3.77 \times 10^{23}$ |
| | 40.7 ± 0.7 | 10.663 | 0.078 | $4.79 \times 10^{-11}$ | 2.81 | $3.68 \times 10^{23}$ |
| $(PANI\ CSA)_{2.0}$ | 75.3 ± 1.7 | 13.626 | 0.057 | $13.85 \times 10^{-11}$ | 2.67 | $4.76 \times 10^{23}$ |
| | 53.0 ± 1.7 | 13.660 | 0.060 | $12.24 \times 10^{-11}$ | 2.68 | $4.75 \times 10^{23}$ |
| | 38.0 ± 0.3 | 11.943 | 0.066 | $7.06 \times 10^{-11}$ | 2.85 | $3.91 \times 10^{23}$ |

### Material and Electrical Characterization

Infrared spectra were obtained on KBr pellets using a Bruker™ Vertex-70 FTIR spectroscope in the range of 4000–400 cm$^{-1}$ with a resolution of 8 cm$^{-1}$. UV–visible spectra were obtained by a PerkinElmer Lambda 35 UV–vis spectrophotometer using a scan speed of 120 nm min$^{-1}$ with data interval of 1 nm in the range of 200–800 nm using a slit width of 0.5 $\mu$m. The elemental analysis was conducted by a Perkin–Elmer CHNS/O analysis kit. The electron paramagnetic resonance of the doped polyaniline films was conducted by using a Bruker EMX EPR spectrometer. The film thicknesses (deposited on glass substrates for this purpose) were measured by an XP 100 stylus profilometer (Ambios Technology). Experiments for film thickness measurements were conducted in duplicate with thickness measurements being conducted at two locations per sample with the error bars representing one standard deviation about the mean. Crystallinity of the PANI EB and PANI CSA powders was examined by XRD (Model ISO Debyeflex 2002). The temperature-dependent DC resistance measurements of the doped polyaniline films were conducted by a two probe method using a Keithley Semiconductor Characterization System (model 4200). Four probe measurements were also carried out by using a Keithley current source (model 2400) and a Keithley voltage measuring setup (2182A) which gave results similar to that of the two probe method. The temperature dependent AC measurements were conducted with an impedance analyzer (Agilent—4294A) in the frequency range of 100 Hz–5 MHz. The surface work function of the polyaniline films was measured by using a Kelvin probe (Kelvin Control 07) having a gold electrode. A hotplate (Corning PC- 600 D) was used to obtain the desired temperature of the samples between 303 and 353 K. The hotplate was set to the desired temperature. The sample was placed on the hotplate with the PET substrate in contact with the plate for a sufficient time for the temperature to stabilize, following which electrical measurements were taken. This was similarly done at different temperatures. The measurements were taken at increasing temperatures and were conducted at a relative humidity of about 65%.

## RESULTS AND DISCUSSIONS

### Material Verification and Characterization

The colors of the solutions of PANI EB in *N*-methyl-2-pyrrolidone (NMP) and PANI CSA in *m*-cresol were deep blue and deep green, respectively, as has been reported in the literature.[20,21] The polymerization of aniline to PANI EB and doping of PANI EB to PANI CSA were verified by comparing the FTIR peaks observed with the peaks reported in the literature.[22,23] Polymerization and doping were also verified by comparing the UV–visible peaks with those reported in the literature.[8,24] The PANI CSA powders were also found to be amorphous (diffractogram not shown) with broad and weak diffraction appearing at $2\theta \approx 10$, 15, and 25 degrees indicating that doping induced a short range ordering in the samples. These diffractograms were similar to those obtained by Saravanan et al.[25]

The film thicknesses used with the different doping contents are shown in Table I. The thickness profile of a typical film (of thickness 64 nm) is shown in Figure 1. The doping levels in the

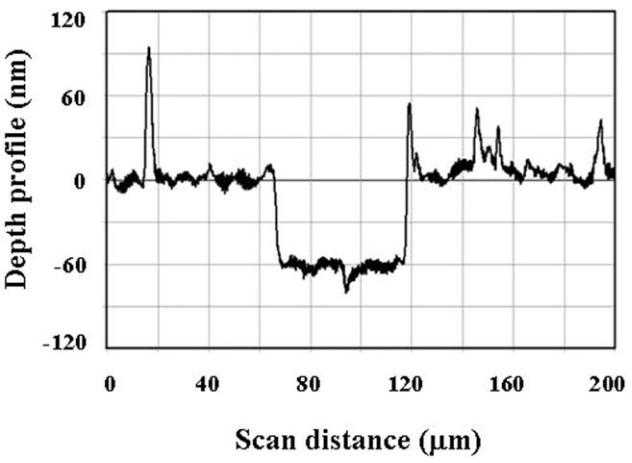


**Figure 1.** Cross-section of a film (obtained from a profilometer) of a film thickness of about 64 nm.

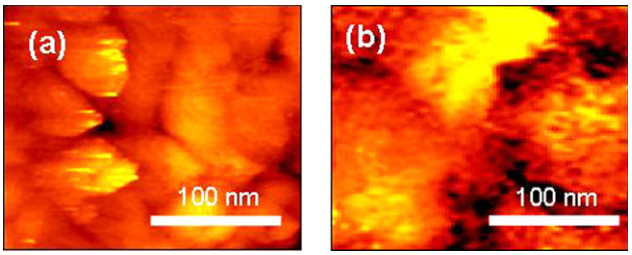


**Figure 2.** STM images of (a) $(PANI\ CSA)_{1.0}$ and (b) $(PANI\ CSA)_{2.0}$ films. [Color figure can be viewed in the online issue, which is available at wileyonlinelibrary.com.]

different films were verified by measuring the sulfur composition as sulfur is only external element present in the dopant not present in the PANI EB prior to doping. The sulfur content was found to be 5.67, 7.41, and 8.70 wt % for the films indicated by $(PANI\ CSA)_{0.6}$, $(PANI\ CSA)_{1.0}$ and $(PANI\ CSA)_{2.0}$ respectively. The different values of sulfur weight percentage present in different doping ratio films also indicated the dopant (CSA) was used in the limiting case, i.e. a saturation level of doping was not reached. The presence of unpaired electrons in the PANI CSA films was indicated by EPR with the *g*-value calculated to be 2.0037, confirming the presence of unpaired electrons in the films responsible for the charge transport.[26] The work function of the films was measured by Kelvin Probe and the values of 4.7–4.8 eV were observed which were in the range reported in the literature,[27] and no significant differences in the work function of the films were observed for the different doping ratios used. Figure 2(a,b) show the STM images of the films for doping ratios of 1 and 2, respectively. The local images show a random distribution of the (darker) conducting and (lighter) insulating regions. The presence of relatively darker regions in the later sample can be attributed to higher doping.

### Electrical Characterization

**DC Measurements.** The films had a linear I–V behavior in the range −4 V to +4 V. The resistance of doped PANI depends on various factors such as the concentration and the nature of dopant, the doping method for PANI EB, the preparation conditions of doped PANI, the PANI morphology (degree of crystallinity) and the influence of the solvent in film formation of doped PANI. We studied the effect of two factors—the doping levels and the film thickness, on the temperature sensitivity of the PANI CSA films. The resistance of the films as a function of temperature with different thicknesses for the samples $(PANI\ CSA)_{0.6}$, $(PANI\ CSA)_{1}$,and $(PANI\ CSA)_{2.0}$ are shown in Figure 3(a–c), respectively. In all cases, the films showed a positive temperature coefficient of resistance with a near linear ($R^2$ values $> 0.9$) resistance versus temperature behavior in the temperature range 303–353 K. This is similar to the behavior shown by metallic films used as temperature sensors but with higher sensitivities as will be seen later. The DC conductivities of the films (ranging from about 2–12 S $cm^{-1}$ depending on doping ratio) are intermediate to those for metallic and semiconducting materials.[28] In the temperature range used, the phonon scattering of the charge carriers dominates over any temperature-assisted hopping transport[5] and this explains the positive temperature coefficient of resistance with temperature. Also, the absolute resistance of the films increased with decrease in the doping level due to lower density of charge carriers, as

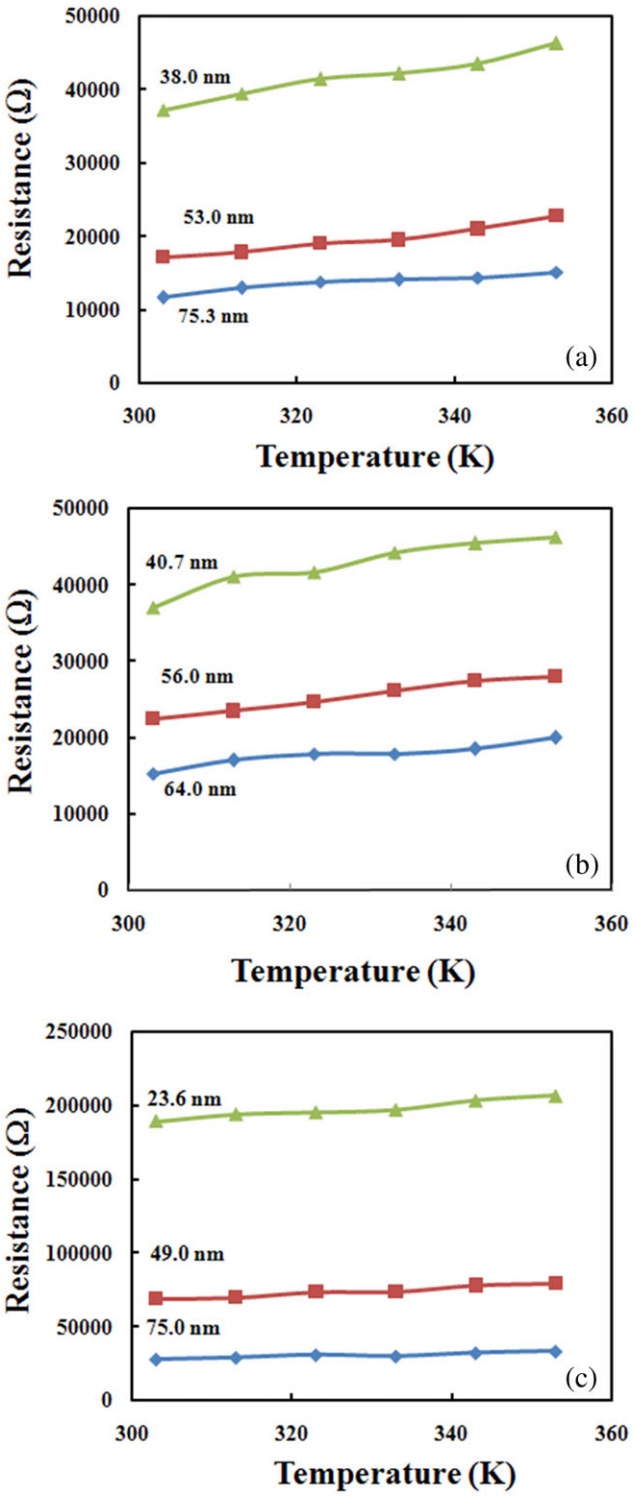


**Figure 3.** Temperature-dependent resistances of (a) $(PANI\ CSA)_{0.6}$ (b) $(PANI\ CSA)_{1.0}$ (c) $(PANI\ CSA)_{2.0}$ films for different film thicknesses. [Color figure can be viewed in the online issue, which is available at wileyonlinelibrary.com.]

Applied Polymer SCIENCE

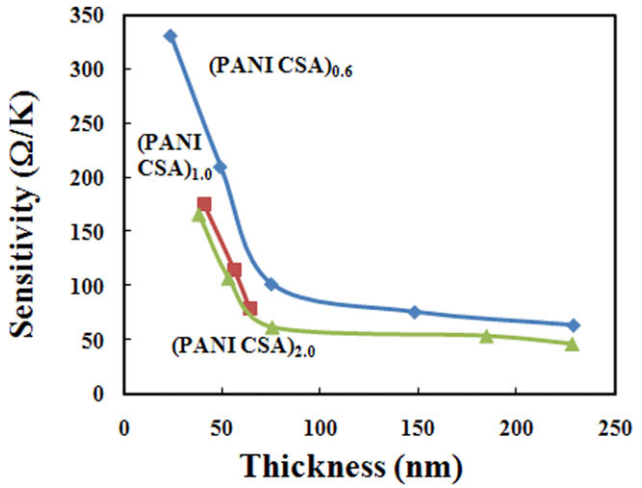


**Figure 4.** Temperature sensitivities of PANI CSA films for different thicknesses and doping levels. High sensitivities are obtained at lower film thicknesses with lower doping levels. [Color figure can be viewed in the online issue, which is available at wileyonlinelibrary.com.]

evidenced from the sulfur content of the films. Films with doping ratios <0.6 were not used as the films did not yield linear I–V curves. For the samples (PANI CSA) $_{0.6}$, the temperature sensitivities (defined as the change in resistance per unit change in temperature), were 102, 210.4, and 331.6 Ω $K^{-1}$ for film thicknesses of 75, 49, and 23.6 nm, respectively; for the samples (PANI CSA) $_{1.0}$, the temperature sensitivities were 80.1, 115.8, and 176 Ω $K^{-1}$ for film thicknesses of 64, 56, 40.7 nm, respectively; and for the samples $(PANI\ CSA)_{2.0}$, the temperature sensitivities were 62.1, 107.4, and 166.2 Ω $K^{-1}$ for the film thicknesses of 75.3, 53, and 38 nm, respectively.

The data from Figure 3(a–c), recast in Figure 4 show the temperature sensitivities as functions of film thicknesses for different doping ratios. For the $(PANI\ CSA)_{0.6}$ and $(PANI\ CSA)_{2.0}$ films, additional results with film thicknesses up to about 240 nm are shown to emphasize the variation of the sensitivities at lower thicknesses. The sensitivity is defined such so as to enable comparison of our films with the commercially available ones.[29] At thicknesses below 80 nm, the sensitivity increases and is strongly affected by the doping level, with decreasing thicknesses. This is seen especially for the doping ratio of 0.6 where sensitivities as high as 330 Ω $K^{-1}$ have been measured. This is a significant result considering that commercial flexible metallic films provide temperature sensitivities ranging from <1 to a maximum of about 10 Ω $°C^{-1}$; with the sensitivities of platinum, copper, nickel, and nickel–iron alloy being in the ranges of 0.39–3.9, 0.04, 0.67–0.81, and 3.13–9.58 Ω $K^{-1}$, respectively.[29] Another important result seen from the above plots is that the temperature sensitivities of these PANI CSA films can be easily tuned as per requirements, which is almost impossible in metallic films where the processing operations are more expensive. To characterize the application of the films on curved surfaces, resistances were measured at various degrees of bending of the film. The films bent manually from 180° (flat condition) to about 80° did not show any appreciable change in the resistance of the films with bending as long as the contacts remained intact. This is an important property which can be utilized for measuring the temperatures on curved surfaces. It is to be noted that the sensitivity can also be defined by other conventions such as change in resistance per unit resistance per unit change in temperature. For the samples $(PANI\ CSA)_{0.6}$, such temperature sensitivities were 5.9 × $10^{-3}$/K, 6.4 × $10^{-3}$/K, and 4.2 × $10^{-3}$/K for film thicknesses of 75, 49, and 23.6 nm, respectively; for the samples $(PANI\ CSA)_{1.0}$, these were 6.2 × $10^{-3}$/K, 4.8 × $10^{-3}$/K, and 4.9 × $10^{-3}$/K for film thicknesses of 64, 56, 40.7 nm, respectively; and for the samples $(PANI\ CSA)_{2.0}$, the temperature sensitivities were 3.9 × $10^{-3}$/K, 2.8 × $10^{-3}$/K, and 1.8 × $10^{-3}$/K for the film thicknesses of 75.3, 53, and 38 nm, respectively. However, as mentioned, we use the definition of resistance change per unit change in temperature to define the sensitivity in this work.

A mechanism for explaining the increase in sensitivity with lower doping levels and decreasing film thickness below 80 nm is proposed. A schematic of the polymer chains with counter-ions is shown in Figure 5, where the doping level increases in the chain from Figure 5(a–c). In these films, the increase in temperature sensitivity can be correlated with the decrease in the film conductivity, seen with decreased doping content and decreasing film thickness. At these ranges of film conductivity, the vibrations of the counter-ions, which can be considered as side chains, affect the vibrations of the main chain which control the charge transport by affecting the level of phonon backscattering of the carriers and hence the conductivity.[16] The chains with a lower doping content, being less bulky, are more responsive to temperature changes in the form of vibrations and thus show higher temperature sensitivities. Also, as seen from Figure 4, for a given doping ratio, the sensitivities increase with the decrease in the thickness. The proportion of chains

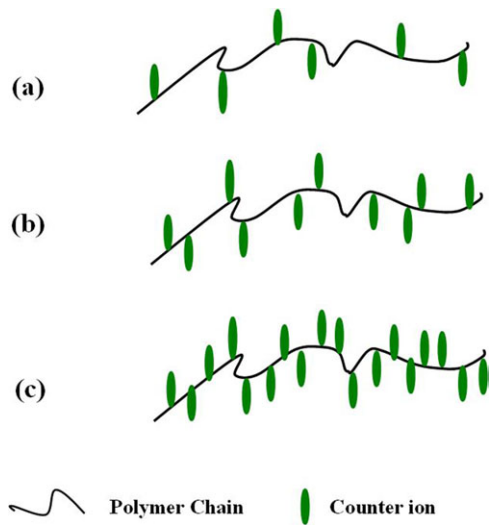


**Figure 5.** Schematic of the proposed model with relatively (a) lower doping (b) relatively moderately doping and (c) relatively higher doping. The chains with relatively lower doping content, being less bulky, are more responsive to the temperature changes in the form of vibrations. [Color figure can be viewed in the online issue, which is available at wileyonlinelibrary.com.]

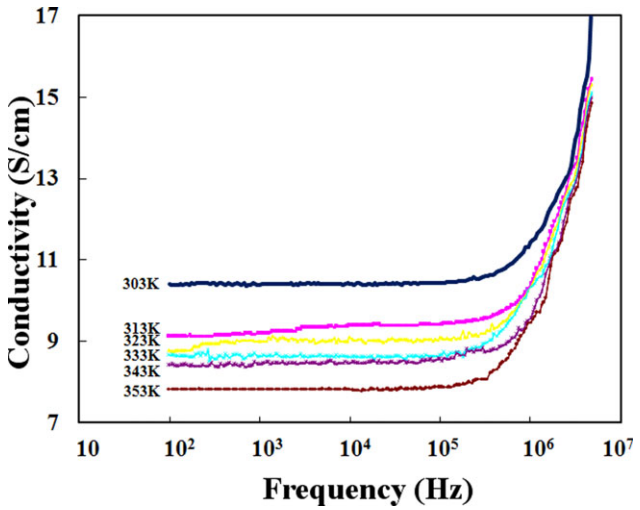


**Figure 6.** AC conductivity as a function of frequency for a (PANI CSA)$_{1.0}$ film of thickness 64 nm in the temperature range 303–353 K. [Color figure can be viewed in the online issue, which is available at wileyonlinelibrary.com.]

near the surface compared to that in the bulk of the film is higher in thinner films. Surface effects play a greater role in modulating the resistance of the films and hence the enhanced sensitivity in thinner films. The effect of film thickness will be further examined from the AC measurement studies in the next subsection.

The phonon frequencies were calculated using the linearized form obtained from expansion of the exponential function in the expression of the film resistivity ($\rho$),[30]

$$\rho = \rho_o e^{-\frac{\hbar\omega_o}{k_B T}} \tag{1}$$

and neglecting the higher order terms. In the above expression, $\rho_o$ is the pre-exponential factor, $\hbar$ is the modified Plank constant, $\omega_o$ is the phonon frequency, $k_B$ is the Boltzmann constant, and $T$ is the absolute temperature. The linearization is justified as the resistance values obtained was almost linear in the temperature range studied. The $\omega_o$ values were calculated as $2.58 \pm 0.18 \times 10^{13}$ Hz, $2.52 \pm 0.05 \times 10^{13}$ Hz, and $1.95 \pm 0.43 \times 10^{13}$ Hz, for the doping ratios of 0.6, 1.0, and 2, respectively. The higher $\omega_o$ values with the lower doping ratios support our proposed mechanism.

**AC Measurements.** AC measurements were conducted to have a better understanding of the charge transport mechanism. The AC conductivity values for films can be described by a power law behavior[31]

$$\sigma(\omega, T) = A\omega^s \tag{2}$$

where $A$ is a constant dependent on temperature, $\omega$ is the angular frequency, and $s$ is the angular frequency index (with $0 < s < 1$). Figure 6 shows the AC conductivity as a function of the frequency, $f$ (with $\omega = 2\pi f$) for a (PANI CSA)$_{1.0}$ film of thickness 64 nm in the temperature range 303–353 K. The conductivity decreased with increasing temperature, as was to be expected from semimetallic films, supporting the DC measurements. The critical frequency, $f_c$, (i.e., the frequency at which the conductivity increases with frequency) decreased with increasing temperature. Similar behavior was seen with the other films (figures not shown). For the same dopant ratio, this frequency increased with increasing film thickness. For similar thicknesses, higher $f_c$ values were observed for films with higher doping levels.

The nature of the temperature dependency of the frequency component $s$ is different in different models (quantum mechanical tunneling, random free energy barrier, correlated barrier hopping, small polaron tunneling). The calculated values of the exponent "$s$" as a function of temperature for the same film (as in Figure 6) are shown in Figure 7, which are seen to increase with increasing temperature thereby possibly indicating a small polaron tunneling (SPT) mechanism. The angular frequency exponent s for such a model is described by Gmati et al.[32]

$$s = 1 + \frac{4}{\ln(\omega\tau_o) + \frac{W_H}{k_B T}} \tag{3}$$

where $k_B$ is the Boltzmann constant, $T$ is the absolute temperature, $W_H$ is the activation energy associated with the electron transfer process between a pair of states, $\tau_o$ is the characteristic relaxation time, and $\omega$ is the angular frequency. Similar behavior was seen in the other films, the plots of which are not shown here.

The best fitted values for $W_H$ and $\tau_o$ values at a frequency of 1 MHz were obtained from the plots of $4/(s-1)$ vs. $1/T$ plots (with $R^2$ values in the range 0.972–0.998) and are shown in Table I. For a given doping ratio, the $W_H$ value increases with decreasing thickness. For example, as seen in the table, for a doping ratio of 0.6, the $W_H$ values are 0.066, 0.091, and 0.099 eV for the films of thicknesses 75, 49, and 23.6 nm, respectively.

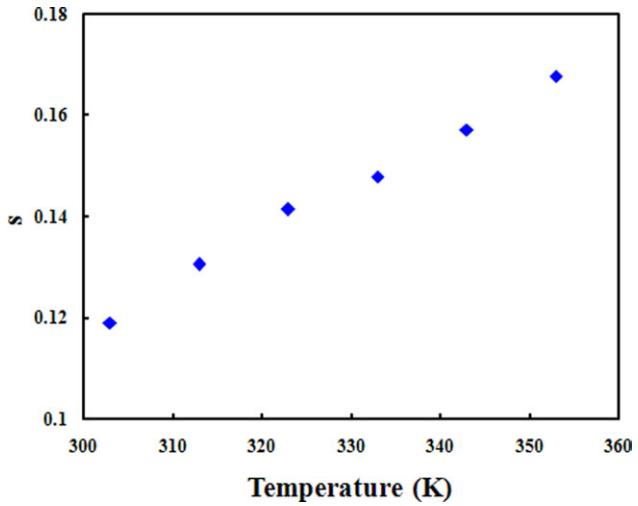


**Figure 7.** The coefficient "$s$" as a function of temperature for a (PANI-CSA)$_{1.0}$ film of thickness 64 nm in the temperature range 303–353 K. [Color figure can be viewed in the online issue, which is available at wileyonlinelibrary.com.]

Similarly, for the doping ratio of 1.0, the $W_H$ values are 0.046, 0.063, and 0.078 eV for the films of thicknesses 64, 56, and 40.7 nm, respectively. And, for the doping ratio of 2.0, the $W_H$ values are 0.057, 0.060, and 0.066 eV for the films of thicknesses 75.3, 53, and 38 nm, respectively. For a given thickness, the $W_H$ value increases with decreasing doping ratio. For example, at a thickness of about 75 nm, the $W_H$ value increases from 0.057 eV for a doping ratio of 2.0, to 0.066 eV for a doping ratio of 0.6. Similarly, for comparable thicknesses of 40.7 and 38 nm, the $W_H$ value increases from 0.066 to 0.078 eV for a decrease in the doping ratio from 2 to 1. The $\tau_o$ values are in the range $10^{-10}$–$10^{-11}$ Hz and for a given doping ratio (with the exception of the doping ratio of 0.6), these values decrease with decreasing film thickness.

$R_{\omega,}$ the tunneling distance at a particular angular frequency $\omega$, is given by[32]:

$$R_\omega = \frac{1}{2\alpha}\left[\ln\left(\frac{1}{\omega\tau_o}\right) - \frac{W_H}{k_B T}\right] \quad (4)$$

where $\alpha$ is the inverse localization length (taken as $\alpha^{-1} = 1.1$ nm) with other terms described earlier. The $R_\omega$ values were in the range 2.5–3.1 nm (shown in Table I) for all films measured at a frequency of 1 MHz.

The density of states at the Fermi level, $N(E_F)$, can be calculated from,[32]

$$\sigma(\omega) = ce^2 k_B T \alpha^{-1}[N_E(F)]^2 \omega {R_\omega}^4 \quad (5)$$

where, $c$ is a constant taken as $\pi^4/24$, $e$ is the electronic charge ($1.602 \times 10^{-19}$ C), and the parameters have been defined previously. As seen in Table I, the $N(E_F)$ values calculated at a frequency of 1 MHz are of the order of $10^{23}$ $eV^{-1}$ $cm^{-3}$. For a given thickness, the $N(E_F)$ values increase with increasing doping ratio. For example, for films of about 75 nm thickness, at a temperature of 303 K, the value increases from $2.71 \times 10^{23}$ $eV^{-1}$ $cm^{-3}$ for a doping ratio of 0.6–$4.76 \times 10^{24}$ $eV^{-1}$ $cm^{-3}$ for a doping ratio of 2.0. This is attributed to increased number charged carriers with higher doping content and increasing $N(E_f)$ values with increased doping content in (thicker) polyaniline films have been reported in the literature.[32] For a given doping ratio, the values decrease with decreasing thickness. For the doping ratio of 0.6, again at 303 K, the values decreased from $2.71 \times 10^{23}$ $eV^{-1}$ $cm^{-3}$ at 75 nm to $2.05 \times 10^{23}$ $eV^{-1}$ $cm^{-3}$ at 23.6 nm, for the doping ratio of 1.0, the values decreased from $4.74 \times 10^{23}$ $eV^{-1}$ $cm^{-3}$ at 64 nm to $3.68 \times 10^{23}$ $eV^{-1}$ $cm^{-3}$ at 40.6 nm, and for the doping ratio of 2.0, the values decreased from $4.76 \times 10^{23}$ $eV^{-1}$ $cm^{-3}$ at 75.3 nm to $3.91 \times 10^{23}$ $eV^{-1}$ $cm^{-3}$ at 38 nm. To the best of our knowledge, we are not aware any other reports on $N(E_f)$ values as a function of the thickness of polyaniline films. The conductivity values, at a temperature of 303 K and a frequency of 1 MHz obtained from experiments, used in the calculations are provided in Table I. The AC conductivity values at a frequency of 1 MHz of the different films, needed for the calculations here are provided in Table I and are obtained from the AC conductivity vs. frequency curves for the different films, one of which is shown in Figure 6.

As is seen from the transport parameters calculated from the AC measurements, for a given thickness, the $W_H$ values decrease and the $N(E_F)$ values increase with increasing doping level, and for a given doping level, the $W_H$ values increase and the $N(E_F)$ values decrease with decreasing film thickness. This behavior is consistent with manifestation of lowering of film conductivity with decreasing doping level and decreasing the film thickness. And these observations support the mechanism proposed to explain observation of higher thermal sensitivity at lower thicknesses and lower doping levels. This suggests that further lowering of the film conductivity could be exploited to obtain higher sensitivities but as mentioned, further lowering of the doping ratio did not yield liner I–V curves which made the definition of resistance difficult. Thus, to use the material as resistive sensors with thermal high sensitivity, the conductivity should be low to obtain high sensitivity while still displaying an ohmic behavior. Thus an optimum window of conductivity is desired to obtain the maximum sensitivity. Two parameters for controlling the conductivity, the doping ratio and film thickness have been investigated here. While the doping ratio can be considered a "coarse" knob, the film thickness in the sub-100 nm dimensions can be considered a "fine" knob. And further lowering of the film thickness can be looked into by considering other deposition methods. While the numbers calculated here have an error associated with them due to contribution from the measurements of the film thicknesses and fitting of the "*s*" parameters, what is of importance is the relative values of these parameters which helps understand the role of the doping content and the film thickness. Further understanding the mechanisms can be looked at by studying the role of the carrier concentrations and the carrier mobilities at a wider range of temperatures and this is a subject of a future work.

Humidity is known to affect the conductivity of these films as water vapor acts as a secondary doping agent.[33] Our experiments were conducted at a controlled humidity of 65%. The effect of humidity on these films is a subject of another work and can be minimized by encapsulation.[34]

## CONCLUSIONS

The thermal sensitivities of the thin (sub-100 nm) PANI CSA films of different thicknesses and doping levels were studied. Higher sensitivities were obtained in thinner films with lower doping levels with variations in sensitivities being more pronounced at lower thicknesses. Sensitivities, based on DC measurements, as high as 330 $\Omega$ $K^{-1}$ were obtained and these are higher than those obtained from commercially available resistive flexible temperature sensors. Also, the sensitivities could be tuned by varying the thickness and the doping level. These films did not show appreciable change in resistance upon bending and thus can be utilized for temperature measurements on curved surfaces. The increase in temperature sensitivities can be correlated with the decrease in the film conductivities, which occur with decreased doping levels and decreased film thicknesses. The increase in sensitivity with lower doping levels and decreasing film thickness could be understood based on the vibrations of the counter-ions affecting the vibrations of the main chain which control the charge transport and thus

affecting the level of phonon backscattering of the carriers, and the relative values of the calculated phonon frequencies support the proposed mechanism. AC studies showed behavior (i.e., decrease in $W_H$ values and increase in $N(E_F)$ values with increasing doping ratio at a given film thickness, and increase in $W_H$ values and decrease in $N(E_F)$ values with decreasing film thickness for a given doping level) consistent with manifestation of lowering of film conductivity with decreasing doping ratio and decreasing the film thickness which support the proposed mechanism to explain the observation of higher thermal sensitivity at lower thicknesses and lower doping ratios.

## ACKNOWLEDGMENTS

The authors gratefully acknowledge the financial support from the Department of Science and Technology (DST), Govt. of India. The STM measurements of the films by Prof. Anjan Gupta are appreciated. The authors thank Prof. Y.N. Mohapatra for use of the impedance analyzer.

## REFERENCES

1. Barth, P. W.; Bernard, S. L.; Angell, J. B. *IEEE Trans. Electron. Dev.* **1985,** *ED-32*, 1202.
2. Moser, Y.; Gijs, M. A. M. *J. Microelectromech. Syst.* **2007,** *16*, 1349.
3. Lee, G. B.; Huang, F. C.; Lee, C. Y.; Miau, J. *J. Acta Mech. Sin. Lixue Xuebao* **2004,** *20*, 140.
4. Kim, S.; Ko, J. M.; Chung, I. J. *Polym. Adv. Technol.* **1996,** *7*, 599.
5. Long, Y.; Chen, Z.; Wang, N.; Zhang, Z.; Wan, M. *Phys. B* **2003,** *325* 208.
6. Ebrahim, S.; Kashyout, A.-H.; Soliman, M. *Curr. Appl. Phys.* **2009,** *9*, 448.
7. Pinto, N. J.; Carrión, P. L.; Ayala, A. M.; Ortiz-Marciales, M. *Synth. Metals* **2005,** *148*, 271.
8. Prakash, T.; Dass, S. A. K. N.; Nazeer, K. P. *Bull. Mater. Sci. Indian Acad. Sci.* **2002,** *25*, 521.
9. Huang, J.; Wan, M. *Solid State Commun.* **1998,** *108*, 255.
10. Bhadra, J.; Sarkar, D. *Mater. Lett.* **2009,** *63*, 69.
11. Dutta, P.; Biswas, S.; Ghosh, M.; De, S. K.; Chatterjee, S. *Synth. Metals* **2001,** *122*, 455.
12. Gupta, K.; Chakraborty, G.; Jana, P. C.; Meikap, A. K. *Solid State Commun.* **2011,** *151*, 573.
13. Sarkar, A.; Ghosh, P.; Meikap, A. K.; Chattopadhyay, S. K.; Chatterjee, S. K.; Ghosh, M. *J. Appl. Phys.* **2005,** *97*, 113713.
14. Bianchi, R. F.; Ferreira, G. F. L.; Lepienski, C. M.; Faria, R. M. *J. Chem. Phys.* **1999,** *110*, 4602.
15. Prem Nazeer, K.; Thamilselvan, M.; Mangalaraj, D.; Narayandass, S.; Yi, J. *J. Polym. Res.* **2006,** *13*, 17.
16. Adams, P. N.; Devasagayam, P.; Pomfret, S. J.; Abell, L.; Monkman, A. P. *J. Phys. Condens. Matter.* **1998,** *10*, 8293.
17. Jin, J.; Wang, Q.; Haque, M. A. *J. Phys. D Appl. Phys.* **2010,** *43*, 205.
18. Jin, J.; Wang, Q.; Haque, M. A. *Org. Electron.* **2010,** *11*, 29.
19. Stejskal, J.; Gilbert, R. G. *Pure Appl. Chem.* **2002,** *74*, 857.
20. Cao, Y.; Smith, P.; Heeger, A. J. *Synth. Metals* **1993,** *57*, 3514.
21. Kuo, C.-T.; Chen, C.-H. *Synth. Metals* **1999,** *99*, 163.
22. Asturias, G. E.; MacDiardmid, A. G. *Synth. Metals* **1989,** *29*, 157.
23. Campos, T. L. A.; Kersting, D. F.; Ferreira, C. A. *Surf. Coat. Technol.* **1999,** *122*, 3.
24. Masters, J. G.; Sun, Y.; Macdiarmid, A. G. *Synth. Metals* **1991,** *41–43*, 715.
25. Saravanan, S.; Joseph Mathai, C.; Anantharaman, M. R.; Venkatachalam, S.; Prabhakaran, P. V. *J. Phys. Chem. Solids* **2006,** *67*, 1496.
26. Altshuler, S. A.; Kozirev, B. M. Electron Paramagnetic Resonance; New York: Academic Press, **1964.**
27. Liess, M.; Chinn, D.; Petelenz, D.; Janata, J. *Thin Solid Films* **1996,** *286*, 252.
28. Callister, W. D. Fundamentals of Materials Science and Engineering; John Wiley and Sons: New York, **2001.**
29. Available at: www.minco.com.
30. Kivelson, S.; Heeger, A. J. *Synth. Metals* **1988,** *22*, 371.
31. Jonscher, A. K. *Nature* **1977,** *267*, 673.
32. Gmati, F.; Fattoum, A.; Bohli, N.; Dhaoui, W.; Mohamed, A. B. *J. Phys. Condens. Matter* **2007,** *19*, 326203.
33. Winokur, M. J.; Mattes, B. R. *Macromolecules* **1998,** *31*, 8183.
34. Dennler, G.; Lungenschmied, C.; Neugebauer, H.; Sariciftci, N. S.; Latrèche, M.; Czeremuszkin, G.; Wertheimer, M. R. *Thin Solid Films* **2006,** *511/512*, 349.